CrossMark

A new mixed finite-element approach for the elastoplastic analysis of Mindlin plates

Akif Kutlu [ORCID] · **Günther Meschke** ·
Mehmet Hakkı Omurtag

Abstract The objective of this paper is to develop an accurate and efficient solution procedure for elastoplastic problems in structural mechanics in the framework of a two-field mixed variational principle. A novel solution algorithm is proposed and applied to the elastoplastic analysis of Mindlin plates. The Hellinger–Reissner principle is adopted to obtain the global finite-element equations of the problem. Instead of a static condensation, the stress-type field variables are preserved during the solution. According to the proposed approach, the strain increments within a nonlinear solution step are obtained directly at the nodal points from matrix operations instead of gradients of a displacement field. In the present implementation, the von Mises yield criterion with linear hardening is adopted. For the integration of the elastoplastic constitutive rate equations at the nodal points, a 3D fully implicit algorithm is employed. A layered approach is followed to enable the resolution of the plastic strains through the plate thickness. The mixed formulation of the Mindlin plate theory is shear-locking free by construction. The proposed solution strategy is verified by solving several benchmark problems that demonstrate the high accuracy and convergence rate of the presented layered mixed formulation for elastoplastic analyses.

Keywords Elastoplastic analysis · Hellinger–Reissner principle · Layered approach · Linear hardening · Mindlin plate · Mixed formulation

Mathematics Subject Classification 74K20 · 74C05 · 74S05

1 Introduction

The finite-element method (FEM) has a long-standing tradition as a versatile and efficient tool for the numerical solution of engineering problems, including problems involving the analysis of the nonlinear behavior of materials

A. Kutlu (✉) · M. H. Omurtag
Civil Engineering Faculty, Istanbul Technical University, Maslak, 34469 Istanbul, Turkey
e-mail: kutluak@itu.edu.tr

M. H. Omurtag
e-mail: omurtagm@itu.edu.tr

G. Meschke
Institute for Structural Mechanics, Ruhr University Bochum, 44780 Bochum, Germany
e-mail: guenther.meschke@ruhr-uni-bochum.de

and structures; see the monographs [1,2]. In standard displacement-based formulations the resulting stress field is, in general, characterized by jumps along interelement boundaries. In the case of lower-order elements, numerical instabilities, such as locking, in the case of (nearly) incompressible materials may be encountered. As an alternative, finite-element formulations based on mixed variational formulations, leading to so-called mixed finite-element formulations, have been proposed and successfully applied to various types of engineering problems [3–5]. Mixed formulations have also been adopted for nonlinear beam, plate, and shell elements [6,7]. In recent decades, a large number of nonlinear mixed variational formulations of beam/column-framed structures have been proposed in particular to avoid computational difficulties associated with displacement-based formulations, for example, [8–11]. Mixed finite-element formulations not only suppress shear and membrane locking problems but also provide accurate stress and displacement quantities with a smaller number of elements [12]. Despite comprehensive studies on both formulations in the literature, the advantages and disadvantages of mixed-type finite elements compared to displacement-type finite elements are still under discussion and the subject of many publications [13,14]. These discussions often focus on algorithms for the updating of the state variables (displacements, rotations, stresses, and stress resultants), which is generally straightforward in displacement-type finite elements but has many alternatives with different complications in mixed finite-element formulations owing to the multiple fields that are introduced, for example, [15]. The proposed mixed finite-element solution strategy involves an efficient procedure for the update of state variables and fully exploits all advantages of mixed variational formulations, for example, introducing shear locking-free analysis and providing a precise stress analysis with fewer elements and less computation time.

A specific focus of this paper is laid on elastoplastic analyses of plate structures using mixed finite elements for Mindlin plates for the purpose of obtaining reliable predictions of the ultimate load. Early attempts to obtain the limit states of structures, for example [16,17], were based on the upper and lower boundary limits [18]. Numerical procedures to determine the limit loads of structures generally requires a discretization of the domain and involves an optimization scheme [19]. As far as thin (shear rigid) plates are concerned, a plastic hinge theory with hardening was employed by Eggers and Kröplin [20] using a mixed finite-element formulation. The elastic–viscoplastic response of Mindlin plates has been investigated by Dinis and Owen [21] with a finite-element formulation based on a yield criterion formulated in terms of stress resultants. A detailed review of elastoplastic finite-element analyses of beam- and plate-type structures was presented by Owen and Hinton [22]. A comprehensive treatment of general geometrically and materially nonlinear problems including plate and shell elements was presented by Bathe and Bolourchi [23]. A semiloof finite element was formulated by Dinis and Owen [24] to incorporate large deflections in the context of elasto-viscoplastic analyses of thin plates and shells in terms of generalized stresses. Reddy and Mitchell [25] applied an extended kinematic minimum principle for the finite-element approximation of Mindlin plates for elastoplastic analyses considering the spread of plasticity through the plate thickness. A layered plate finite element, based on the Hu–Washizu variational principle, was employed by Wempner and Chao–Meng [26] to investigate the propagation of plasticity through the plate thickness using an elastic perfectly plastic material model. In the mixed formulation a constant distribution of the stress resultants was assumed over each plate finite element.

The Hu–Washizu variational principle was taken as the basis for a finite-element model for elastoplastic bending analyses of Reissner–Mindlin plates in Papadopoulos and Taylor [27] using the stress resultant plasticity approach. Daye and Toridis [28] developed a mixed finite-element solution procedure based on the Hellinger–Reissner variational principle using a stress resultant plasticity model for the analysis of the static and dynamic elastoplastic response of shear deformable plate and shallow shell structures taking into consideration the geometrical nonlinearity. A monolithic solution strategy, in conjunction with a tangent stiffness approach to static analysis and an initial stiffness approach to dynamic analysis, was adopted. Papadopoulos and Taylor [29] employed a mixed triangular shear deformable plate element based on the Hu–Washizu variational principle for elasto-viscoplastic analysis of plates using a stress resultant plasticity formulation. In Ibrahimbegović and Frey [30], the enhanced assumed strain method was used to overcome shear locking in a stress resultant plasticity model for shear deformable plates employing a four-node plate finite element. A single scalar equation to update the material state was used for the analyses of plates with different shapes subjected to point and distributed loadings. Auricchio and Taylor [31]

suggested a new elastoplastic shear deformable plate theory by modifying the yield function to make it possible to describe the spread of plasticity through the plate thickness while employing the stress resultant plasticity approach in the finite-element formulation. The advantages and accuracy of this approach were evaluated using comparisons with results from 3D finite-element models and classical elastoplastic plate models.

A mixed finite-element approach using stress resultant plasticity and first-order shear deformation theory was proposed by Croce et al. [32]. In this model, after performing static condensation, only translations and rotations at the nodes were used as field variables. More recently, numerical discretization techniques were proposed to provide an improved resolution that can eliminate shear locking. Rabczuk et al. [33] introduced a meshfree method to analyze the dynamic fracture of thin shells interacting with fluids by covering both the geometric and the material nonlinearities. Areias and Rabczuk [34] used a meshfree method with C^1 continuity on the basis of edge rotations and load control to solve the finite-strain fracture of plates and shells with both brittle and ductile material formulations. A consistent mixed quadrilateral shell element with in-plane shear strains assumed in the scheme of least-squares was suggested by Areias et al. [35] for solving geometrically and materially nonlinear problems. The so-called alpha FEM proposed in [36], which is conceptually based on the node-based smoothed FEM, was applied to laminated composite plates in [37] in conjunction with the discrete gap technique to eliminate shear locking. Furthermore, discretization methods with higher-order approximations, such as the isogeometric method and defining the transverse shear stresses with higher-order theories [38], are suitable candidates for efficient nonlinear analyses of plates.

The main objective of this paper is to develop an efficient mixed finite-element solution algorithm for materially nonlinear finite-element analysis with a specific implementation for elastoplastic analyses of Mindlin plates. To this end, Mindlin plates are formulated within the framework of a two-field mixed variational formulation using a layered approach and a 3D J2-plasticity model with linear hardening. In conventional approaches to mixed finite-element models, a static condensation procedure (on the element or the system level) is performed to restrict the solution of the finite-element equations in terms of the related displacement quantities, which makes it possible to use suitable displacement-based finite-element programs. In contrast to the bulk of existing mixed variational formulations in the literature, a monolithic solution strategy is proposed in this paper, where the stress-type field variables are preserved in addition to the displacement-type field variables. As is demonstrated in the paper, this choice provides several advantages with respect to the numerical formulation. First, all field variables (including displacement- and stress-type variables) are interpolated independently, which relaxes the necessity of satisfying further continuity conditions. Therefore, C^0 continuity is sufficient for the compatibility requirements of the interpolation functions. Stress-type field variables (or their increments) at the finite-element nodes are obtained from the direct solution of the system equations. A continuous distribution of displacement- and stress-type field variables is automatically achieved over the plate domain. Once the stress-type field variables are obtained, compliance matrices are used to compute the strains (or increments of strains) directly at each node, conforming with a continuous strain field over the domain. More importantly, this approach avoids error-prone numerical differentiation operations in the postprocessing phase. An additional advantage of the proposed mixed formulation is that it provides a priori shear-locking-free formulation and that the element performance is independent of the aspect ratio [39].

2 Formulation

2.1 Hellinger–Reissner principle

The Hellinger–Reissner principle [40] defines the total strain energy of a deformable body over a corresponding volume V using the complementary energy $\chi(\sigma)$ as

$$\Pi_{\text{int}} = \int_V W \, dV = \int_V \left(\sigma \varepsilon^{\mathbf{u}} - \chi(\sigma) \right) dV. \tag{1}$$

Here the superscript u symbolizes that the strain tensor $\varepsilon^{\mathbf{u}}$ is defined in terms of displacement components. The Hellinger–Reissner variational principle states that $\delta \Pi_{\text{HR}} = \delta (\Pi_{\text{int}} + \Pi_{\text{ext}}) = 0$, where $\Pi_{\text{ext}}(u)$ is the external
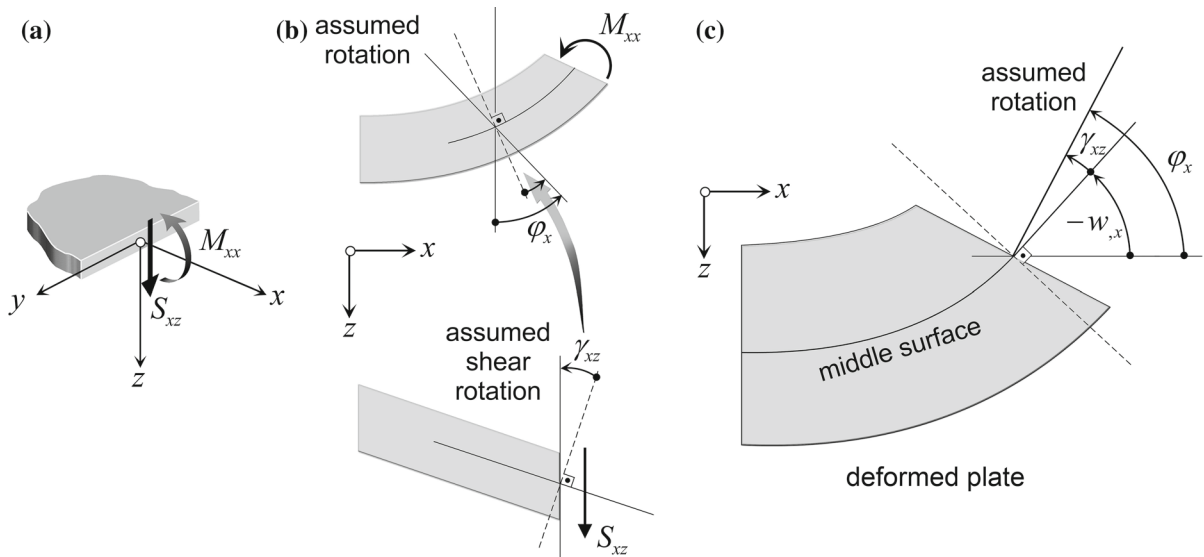
(a) **(b)** assumed rotation **(c)**

Fig. 1 Stress resultants and kinematics according to Mindlin assumptions. **a** Transverse shear force and bending moment on cross section with normal x. **b** Separate rotations of cross section due to bending and transverse shear. **c** Assumed total rotation of cross section

energy. Using Eq. (1), the stationarity of the functional Π_{HR} leads to

$$\delta \Pi_{\mathrm{HR}} = \int_V \left(\sigma \delta \varepsilon^{\mathbf{u}} + \delta \sigma \varepsilon^{\mathbf{u}} - \frac{\partial \chi(\sigma)}{\partial \sigma} \delta \sigma \right) \mathrm{d}V + \delta \Pi_{\mathrm{ext}}(\mathbf{u}) = 0. \tag{2}$$

Using matrix notation, the first variation of the external energy may be expressed as

$$\delta \Pi_{\mathrm{ext}} = \int_V \left(-\mathbf{q}^{\mathrm{T}} \delta \mathbf{u} \right) \mathrm{d}V - \int_{\Gamma_\sigma} \hat{\mathbf{t}}^{\mathrm{T}} \delta \mathbf{u} \, \mathrm{d}\Gamma_\sigma = 0. \tag{3}$$

Here $\mathbf{q}$ denotes the external load vector and $\hat{\mathbf{t}}$ the traction vector at the Neumann boundary Γ_σ of the domain. Considering $\varepsilon = \partial \chi(\sigma)/\partial \sigma$ and rearranging (2) in matrix form exposes the first variation of the Hellinger–Reissner functional as follows:

$$\delta \Pi_{\mathrm{HR}} = \int_V \left(\varepsilon^{\mathbf{u}} - \varepsilon^{\sigma} \right)^{\mathrm{T}} \delta \sigma \, \mathrm{d}V + \int_V \left(\sigma^{\mathrm{T}} \delta \varepsilon^{\mathbf{u}} - \mathbf{q}^{\mathrm{T}} \delta \mathbf{u} \right) \mathrm{d}V - \int_{\Gamma} \hat{\mathbf{t}}^{\mathrm{T}} \delta \mathbf{u} \, \mathrm{d}\Gamma = 0. \tag{4}$$

2.2 Field equations of Mindlin plates

This subsection contains a brief summary of the governing equations of the Mindlin plate theory. The Mindlin plate theory assumes that shear strains $\varepsilon_s = (\gamma_{xz} \quad \gamma_{yz})^{\mathrm{T}}$ are constant through the plate thickness with the related kinematic relations defined as $\gamma_{xz} = w_{,x} + \varphi_x$ and $\gamma_{yz} = w_{,y} + \varphi_y$, respectively. The transverse displacement of the midplane w is positive when it coincides with the positive z-axis. φ_x and φ_y are independent rotation angles of the plate cross sections (Fig. 1). Throughout the paper, the notion $(\ldots)_{,x}$ is used to denote partial derivatives $\partial(\ldots)/\partial x = (\ldots)_{,x}$. The in-plane strains $\varepsilon_f = (\varepsilon_{xx} \quad \varepsilon_{yy} \quad \gamma_{xy})^{\mathrm{T}}$ at any point z on the cross section are calculated from $\varepsilon_f = z\kappa$ (the subscript f denotes quantities associated with flexure), where the curvatures $\kappa = (\kappa_{xx} \quad \kappa_{yy} \quad \kappa_{xy})$ are defined as $\kappa_{xx} = \varphi_{x,x}$, $\kappa_{yy} = \varphi_{y,y}$, and $\kappa_{xy} = \varphi_{x,y} + \varphi_{y,x}$. To trace the spread of the plastic zone through the plate thickness, the cross section is divided into layers (Fig. 2b). Each layer may have individual material properties. Flexural (in-plane) stresses $\sigma_f = (\sigma_{xx} \quad \sigma_{yy} \quad \sigma_{xy})^{\mathrm{T}}$ and transverse shear stresses $\sigma_s = (\sigma_{xz} \quad \sigma_{yz})^{\mathrm{T}}$ are related to their strain counterparts as $\sigma_f = \mathbf{Q}_f \varepsilon_f$ and $\sigma_s = \mathbf{Q}_s \varepsilon_s$ (the subscript s denotes quantities associated with transverse shear).
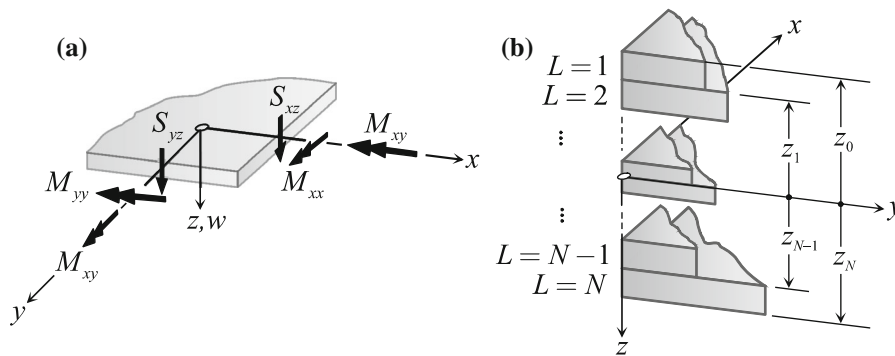
Fig. 2 Layered Mindlin plate. **a** Positive directions of stress resultants. **b** Decomposition of cross section into layers

The flexural and shear parts of the elasticity matrices $\mathbf{Q}_f$ and $\mathbf{Q}_s$ are given as

$$
\mathbf{Q}_f = \begin{pmatrix} Q_{11} & Q_{12} & 0 \\ Q_{21} & Q_{22} & 0 \\ 0 & 0 & Q_{33} \end{pmatrix}, \quad \mathbf{Q}_s = k_s \begin{pmatrix} Q_{44} & 0 \\ 0 & Q_{55} \end{pmatrix}, \tag{5}
$$

with the components $Q_{11} = Q_{22} = E/(1 - \upsilon^2)$, $Q_{12} = Q_{21} = \upsilon E/(1 - \upsilon^2)$, and $Q_{33} = Q_{44} = Q_{55} = G$ and the shear correction factor $k_s = 5/6$. Here, E is the elasticity modulus, υ is Poisson's ratio, and G denotes the shear modulus. Integrating the stresses along the thickness h of the plate by dividing the cross section into N layers yields the stress resultants $\mathbf{M} = (\begin{matrix} M_{xx} & M_{yy} & M_{xy} \end{matrix})^T$ and $\mathbf{S} = (\begin{matrix} S_{xz} & S_{yz} \end{matrix})^T$ as

$$
\mathbf{M} = \int_{-h/2}^{h/2} \boldsymbol{\sigma}_f z \, \mathrm{d}z = \sum_{L=1}^{N} \int_{z_{L-1}}^{z_L} \boldsymbol{\sigma}_f z \, \mathrm{d}z, \quad \mathbf{S} = \int_{-h/2}^{h/2} \boldsymbol{\sigma}_s \, \mathrm{d}z = \sum_{L=1}^{N} \int_{z_{L-1}}^{z_L} \boldsymbol{\sigma}_s \, \mathrm{d}z. \tag{6}
$$

The positive directions of shear forces and moments are defined according to Fig. 2a.

Inserting the constitutive relations into Eq. (6), the stress resultants can be expressed in terms of strains as $\mathbf{M} = \mathbf{D}\boldsymbol{\varepsilon}_f$ and $\mathbf{S} = \mathbf{C}\boldsymbol{\varepsilon}_s$, where the elasticity matrices $\mathbf{D}$ and $\mathbf{C}$ are given explicitly as

$$
D_{ij} = \frac{1}{3} \sum_{L=1}^{N} (Q_{ij})_L (z_L^3 - z_{L-1}^3), \qquad C_{ij} = \sum_{L=1}^{N} (Q_{ij})_L k_s (z_L - z_{L-1}),
$$

respectively. Finally, the equilibrium equations of the Mindlin plate are given as

$$
q_z + S_{xz,x} + S_{yz,y} = 0, \qquad M_{xx,x} + M_{xy,y} - S_{xz} = 0, \qquad M_{yy,y} + M_{xy,x} - S_{yz} = 0.
$$

2.3 Algorithm for elastoplastic analysis of Mindlin plates with mixed finite elements

The FEM is characterized by a spatial discretization of domain $\mathfrak{B}$ as $\mathfrak{B} = \bigcup_{e=1}^{n_{elm}} \mathfrak{B}_e$ (e: element number, n_{elm}: total number of elements), using elementwise approximations of the field variables $\mathbf{x}$ as $\mathbf{x}_e = \sum_{m=1}^{n_{nodes}^e} \phi^m \mathbf{x}_m$ (m: node number, n_{nodes}^e: total number of nodes in an element, ϕ^m: shape functions), and enforcing equilibrium based on an underlying variational principle. In the numerical solution of nonlinear problems, the equilibrium states $\mathbf{F}_{n+1}^{int} = \mathbf{F}_{n+1}^{ext}$ are obtained at discrete load levels ($n+1 = 1, 2, \ldots, NT$) using an iterative solution scheme, such as the Newton–Raphson method. Adopting the Hellinger–Reissner variational principle, equilibrium and constitutive relations are satisfied in a weak form within a two-field formulation, where stresses $\boldsymbol{\sigma}$ and displacements $\mathbf{u}$ are the fundamental variables of the functional.

In this paper, we propose a monolithic solution strategy to iteratively compute the increments of stresses $\Delta\boldsymbol{\sigma}$ and displacements $\Delta\mathbf{u}$ from the solution of the system equations during subsequent Newton steps within a load step
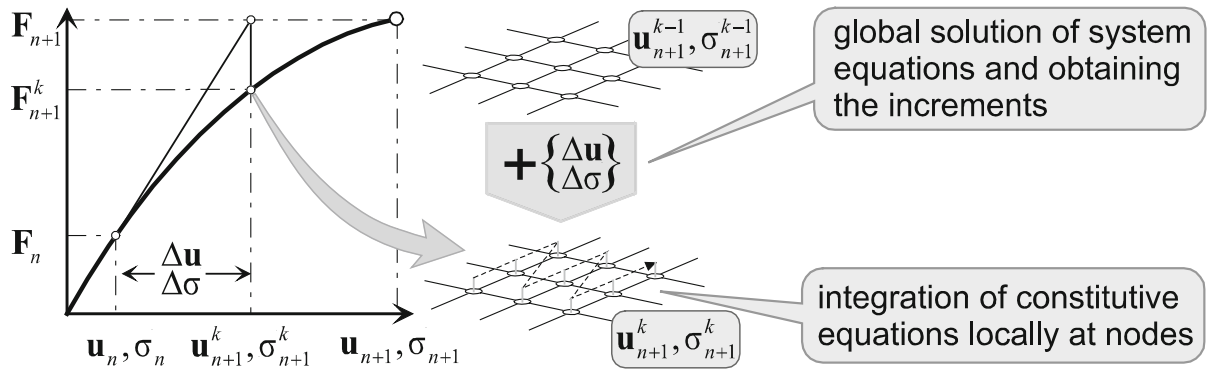
Fig. 3 Overview of proposed elastoplastic algorithm. k is the global iteration step number

$[n, n+1]$ (Fig. 3). During a Newton iteration step k the updated displacements are calculated as $\mathbf{u}_{n+1}^{k} = \mathbf{u}_{n+1}^{k-1} + \Delta\mathbf{u}$. We propose to determine the strain increments $\Delta\boldsymbol{\varepsilon}$ from the tangential relation $\Delta\boldsymbol{\varepsilon} = (\mathbf{C}^{\mathrm{ep}})^{-1}\Delta\boldsymbol{\sigma}$ and to perform the update of the total strains as $\boldsymbol{\varepsilon}_{n+1}^{k} = \boldsymbol{\varepsilon}_{n+1}^{k-1} + \Delta\boldsymbol{\varepsilon}$. From $\boldsymbol{\varepsilon}_{n+1}^{k}$ and the stored values of plastic strains $\boldsymbol{\varepsilon}_{n+1}^{(k-1)p}$ the updated stresses $\boldsymbol{\sigma}_{n+1}^{k}$ are determined from the local integration of the constitutive equations to compute the updated vector of internal forces $\mathbf{F}_{n+1}^{(k)\mathrm{int}}$.

As far as the computational costs of mixed finite-element approaches are concerned, it is evident that the number of degrees is larger compared with displacement-based finite elements. However, while the stresses are calculated from gradients of the displacements in displacement-type elements, connected by a larger numerical error compared to the nodal variables obtained from the solution to the system equations, they are directly computed as field variables in a mixed formulation. Hence, for the same accuracy of the stresses, a smaller number of elements is needed if mixed elements are used. In addition, it should be pointed out that the proposed solution algorithm provides the following significant additional advantages:

1. The strain increments $\Delta\boldsymbol{\varepsilon}$ can be calculated either from the displacement gradient (as in the displacement method) or from the stress increments $\Delta\boldsymbol{\sigma}$ via the compliance matrices (as in a mixed formulation). Clearly, the latter approach is more precise. Compared to the numerical differentiation using matrix operations to calculate strain increments as required in the displacement approach, it is more efficient in terms of computation time.
2. Since the stress increments $\Delta\boldsymbol{\sigma}$ are calculated at each nodal point of a domain directly from the global equation system, the strain increments $\Delta\boldsymbol{\varepsilon}$ are also computed at each node. Therefore, local constitutive integration can be performed at the nodes of the domain instead of the elements' Gaussian points. The total calculation time related to the constitutive routine is proportional to the total number of nodal points, which is less than the total number of Gaussian points within the mesh.
3. Displacement-type finite-element formulations perform local constitutive integrations at the Gaussian points, which may lead to discontinuous plastic zones within the analysis domain. One Gaussian point may become plastic within a load increment, while the other nearby Gaussian points may be still in an elastic regime. In contrast, the proposed algorithm for integrating constitutive relations at nodal points exploits the fact that the stresses – and, consequently, the material behavior – is continuous over the domain. The proposed algorithm is summarized in Table 1.

2.3.1 Algorithm for mixed elastoplastic finite-element analysis of layered Mindlin plates

In this subsection the proposed general two-field finite-element formulation for elastoplastic analysis is adapted to Mindlin plates. To this end, instead of stresses, stress resultants **P** are used. Nodal displacements and rotations are summarized in vector **u** and curvatures and shear deformations in vector **e**. Referring to definition (4), the first

Table 1 Algorithm for materially nonlinear two-field mixed finite elements

n load step counter, NT total number of load steps, k global iteration counter, $KONV$ limit for global iteration, nd counter for nodes, TND total number of nodes

Loop over load steps $(n = 0,\ NT - 1)$:
  Compute external load vector at $n + 1$: $\mathbf{F}_{n+1}^{\text{ext}}$
  Initialize: $\mathbf{u}_{n+1}^{0} = \mathbf{u}_{n}$
  Iteration step loop $(k = 0,\ KONV)$:
    Compute tangent material matrices: $\mathbf{C}^{\text{ep}}$
    Generate tangent system matrix: $\mathbf{K}_{t}$
    Calculate the increments: $\Delta\mathbf{u}, \Delta\boldsymbol{\sigma} = \mathbf{K}_{t}^{-1}\left(\mathbf{F}_{n+1}^{\text{ext}} - \mathbf{F}_{n+1}^{(k)\,\text{int}}\right)$
    Update displacements: $\mathbf{u}_{n+1}^{k+1} = \mathbf{u}_{n+1}^{k} + \Delta\mathbf{u}$
    Loop over nodes in the domain $(nd = 1,\ TND)$:
      Compute the strain increments: $\Delta\boldsymbol{\varepsilon}^{k} = \mathbf{C}_{\text{tan}}^{-1}\Delta\boldsymbol{\sigma}$
      Update total the strains: $\boldsymbol{\varepsilon}_{n+1}^{k+1} = \boldsymbol{\varepsilon}_{n+1}^{k} + \Delta\boldsymbol{\varepsilon}^{k}$
      Call constitutive integration algorithms and calculate stresses and other state variables: $\boldsymbol{\sigma}_{n+1}^{k+1},\ \boldsymbol{\alpha}_{n+1}^{k+1},\ \boldsymbol{\varepsilon}_{n+1}^{(k+1)p}$
    Compute internal force vector: $\mathbf{F}_{n+1}^{(k+1)\,\text{int}}(\boldsymbol{\sigma}_{n+1}^{k+1})$
    Check for convergence:

variation of the Hellinger–Reissner functional for Mindlin plates is given as

$$\delta\Pi_{\text{HR}} = \int_{\Omega}\left(\mathbf{e}^{\mathbf{u}} - \mathbf{e}^{\mathbf{P}}\right)^{\text{T}}\delta\mathbf{P}\,\mathrm{d}\Omega + \int_{\Omega}\left(\mathbf{P}^{\text{T}}\delta\mathbf{e}^{\mathbf{u}} - \mathbf{q}^{\text{T}}\delta\mathbf{u}\right)\mathrm{d}\Omega = 0, \tag{7}$$

where Ω defines the middle plane of the plate as the integral domain. The notations $\mathbf{e}^{\mathbf{u}}$ and $\mathbf{e}^{\mathbf{P}}$ represent curvatures and transverse shear strains in terms of displacements and stress resultants, respectively. Inserting the compatibility and equilibrium equations from Sect. 2.2, Eq. (7) can be reformulated as

$$\begin{aligned}
\delta\Pi_{\text{HR}} = &\int_{\Omega}\left[\varphi_{x,x} - \left(D_{11}^{-1}M_{xx} + D_{12}^{-1}M_{yy}\right)\right]\delta M_{xx}\,\mathrm{d}\Omega \\
&+ \int_{\Omega}\left[\varphi_{y,y} - \left(D_{21}^{-1}M_{xx} + D_{22}^{-1}M_{yy}\right)\right]\delta M_{yy}\,\mathrm{d}\Omega \\
&+ \int_{\Omega}\left[\varphi_{x,y} + \varphi_{y,x} - D_{33}^{-1}M_{xy}\right]\delta M_{xy}\,\mathrm{d}\Omega + \int_{\Omega}\left[w_{,x} + \varphi_{x} - C_{11}^{-1}S_{xz}\right]\delta S_{xz}\,\mathrm{d}\Omega \\
&+ \int_{\Omega}\left[w_{,y} + \varphi_{y} - C_{22}^{-1}S_{yz}\right]\delta S_{yz}\,\mathrm{d}\Omega + \int_{\Omega}\left[S_{xz}\delta w_{,x} + S_{yz}\delta w_{,y}\right]\mathrm{d}\Omega \\
&+ \int_{\Omega}\left[M_{xx}\delta\varphi_{x,x} + M_{xy}\delta\varphi_{x,y} + S_{xz}\delta\varphi_{x}\right]\mathrm{d}\Omega + \int_{\Omega}\left[M_{xy}\delta\varphi_{y,x} + M_{yy}\delta\varphi_{y,y} + S_{yz}\delta\varphi_{y}\right]\mathrm{d}\Omega \\
&- \int_{\Omega}\delta w q_{z}\,\mathrm{d}\Omega = 0.
\end{aligned} \tag{8}$$

The functional can be linearized about the current state at iteration step k as $L[\delta\Pi_{\text{HR}}] = \delta\Pi_{\text{HR}}^{k} + \Delta\delta\Pi_{\text{HR}}^{k}$, where $\delta\Pi_{\text{HR}}^{k} = \delta\Pi_{\text{HR}}\left(\mathbf{u}^{k}, \mathbf{P}^{k}, \delta\mathbf{u}, \delta\mathbf{P}\right)$ defines the state of the system at iteration step k depending on the state variables $\mathbf{u}^{k}, \mathbf{P}^{k}$. Considering geometrically linear problems, because the compatibility relations are ensured $\mathbf{e}^{\mathbf{u}^{k}} - \mathbf{e}^{\mathbf{P}^{k}} = \mathbf{0}$ in state k, where the strains are fixed, the determination of the state of displacements, rotations, and stress resultants is only related to the satisfaction of the equilibrium of the system,

$$\begin{aligned}
\delta\Pi_{\text{HR}}^{k} &= \int_{\Omega}\underbrace{\left(\mathbf{e}^{\mathbf{u}^{k}} - \mathbf{e}^{\mathbf{P}^{k}}\right)^{\text{T}}}_{0}\delta\mathbf{P}\,\mathrm{d}\Omega + \int_{\Omega}\left(\mathbf{P}^{(k)\text{T}}\delta\mathbf{e}^{\mathbf{u}^{k}} - \mathbf{q}^{\text{T}}\delta\mathbf{u}\right)\mathrm{d}\Omega \\
&= \int_{\Omega}\left(\mathbf{P}^{(k)\text{T}}\delta\mathbf{e}^{\mathbf{u}^{k}} - \mathbf{q}^{\text{T}}\delta\mathbf{u}\right)\mathrm{d}\Omega,
\end{aligned} \tag{9}$$

Table 2 Algorithm for materially nonlinear analysis for Mindlin plates using mixed finite elements

Loop over load steps $(n = 0,\ NT - 1)$:

    Compute external load vector at $n + 1$ Generate external load: $\overset{+}{\mathbf{F}}{}^{\,\text{ext}}_{n+1}$

    Initialize: $\mathbf{u}^{0}_{n+1} = \mathbf{u}_{n}$

    Iteration step loop $(k = 0,\ KONV)$:

        Compute tangent material matrices: $\mathbf{C}^{\text{ep}}$

        Generate tangent system matrix: $\overset{++}{\mathbf{K}}{}^{\,k}$

        Compute the increments: $\Delta\mathbf{u}, \Delta\mathbf{P} = \left(\overset{++}{\mathbf{K}}{}^{\,k}\right)^{-1}\left(\overset{+}{\mathbf{F}}{}^{\,\text{ext}}_{n+1} - \overset{+}{\mathbf{F}}{}^{\,k(\text{int})}_{n+1}(\mathbf{P}^{k}_{n+1})\right)$

        Update displacements: $\mathbf{u}^{k+1}_{n+1} = \mathbf{u}^{k}_{n+1} + \Delta\mathbf{u}$

        Loop over nodes in the domain $(nd = 1,\ TND)$:

            Compute increments in curvatures and shear strains at
            the node nd : $\Delta\mathbf{e}(\Delta\mathbf{P})$

            Loop over layers $(L = 1, N)$:

                Compute strain increment: $\Delta\boldsymbol{\varepsilon}^{k}(\Delta\mathbf{e})$

                Update total strains: $\boldsymbol{\varepsilon}^{k+1}_{n+1} = \boldsymbol{\varepsilon}^{k}_{n+1} + \Delta\boldsymbol{\varepsilon}^{k}$

                Call constitutive integration algorithms and
                calculate stresses and other state variables: $\boldsymbol{\sigma}^{k+1}_{n+1}$,
                $\boldsymbol{\alpha}^{k+1}_{n+1}$, $\boldsymbol{\varepsilon}^{(k+1)p}_{n+1}$

        Compute internal force vector: $\overset{+}{\mathbf{F}}{}^{\,k+1(\text{int})}_{n+1}(\mathbf{P}^{k+1}_{n+1})$

        Check for convergence:

which, after inserting approximations, generates the global state vector (or internal force vector) $\overset{+}{\mathbf{F}}{}^{\,k(\text{int})}$ and external load vector $\overset{+}{\mathbf{F}}{}^{\,\text{ext}}$ in the form $\overset{+}{\mathbf{F}}{}^{\,k(\text{int})} - \overset{+}{\mathbf{F}}{}^{\,\text{ext}}$. Here $\mathbf{P}^{k}$ is the vector of the stress resultants at state k calculated from the integrals of stresses obtained from the local integration of the constitutive equations. The increments of the displacements and rotations $\Delta\mathbf{u}$ and of the stress resultants $\Delta\mathbf{P}$ are computed from the solution of the global system of equations. The tangent system matrix is generated according to the directional derivative of the first variation of the functional:

$$\Delta\delta\Pi^{k}_{\text{HR}} = \lim_{\beta\to 0}\left(\frac{\mathrm{d}}{\mathrm{d}\beta}[\delta\Pi_{\text{HR}}(\mathbf{u} + \beta\mathbf{u}, \mathbf{P} + \beta\mathbf{P}, \delta\mathbf{u}, \delta\mathbf{P})]_{(\mathbf{u}=\mathbf{u}^{k}, \mathbf{P}=\mathbf{P}^{k})}\right). \tag{10}$$

Considering only material nonlinearity, (10) yields

$$\Delta\delta\Pi^{k}_{\text{HR}} = \int_{\Omega}\left[\Delta\mathbf{e}^{\mathbf{u}}\delta\mathbf{P} - \overline{\mathbf{D}}^{-1}_{k}\Delta\mathbf{P}\delta\mathbf{P} + \Delta\mathbf{P}\delta\mathbf{e}^{\mathbf{u}}\right]\mathrm{d}\Omega,$$

which, after including finite-element approximations, corresponds to the structural tangent matrix $\overset{++}{\mathbf{K}}$. $\overline{\mathbf{D}}^{-1}_{k} = (\mathrm{d}\mathbf{e}^{\mathbf{s}}/\mathrm{d}\mathbf{s})|^{k}$ is the section compliance matrix at iteration step k, which is calculated by integrating the tangent elastoplastic moduli of each layer through the thickness of the plate. The section compliance matrices are generated at nodes and interpolated over the finite elements as

$$\overline{D}^{-1}_{ij} = \sum_{m=1}^{n^{e}_{\text{nodes}}}\phi^{m}(\overline{D}^{m}_{ij})^{-1}, \tag{11}$$

where $(\overline{D}^{m}_{ij})^{-1}$ is the section compliance matrix computed at node m, ϕ^{m} is the corresponding shape function, and Σ represents the assembly operator. The proposed algorithm for the elastoplastic analyses of Mindlin plates is summarized in Table 2.

2.3.2 Computation of transverse shear strains

Assuming a constant shear strain according to the Mindlin plate theory yields an inexact stress distribution, although the shear forces are calculated adequately through the mixed formulation. To avoid this deficiency, the transformed

section method, or equivalent section method [41,42], is adopted. This method entails a continuous distribution of the shear strains and uses effective section properties to determine the transverse stress distribution through the plate thickness. The proposed mixed formulation provides the required shear forces directly, which is an additional advantage for the postprocessing phase.

2.3.3 Finite-element discretization

Quadrilateral isoparametric finite elements are used to discretize the plate domain. Each node has eight field variables corresponding to both displacements and rotations as well as to stress resultants: w, φ_x, φ_y, S_{xz}, S_{yz}, M_{xx}, M_{yy}, M_{xy}. Since functional (8) only contains first-order derivatives, linear shape functions are sufficient to fulfill the C^0 continuity requirement. The evaluation of the integrals is performed by means of a 2×2 Gaussian quadrature scheme.

2.4 Numerical integration of elastoplastic constitutive equations

For the integration of the elastoplastic equations, a predictor–corrector scheme with the now standard return mapping algorithm [43,44] is employed. For completeness, only a brief summary is given in this subsection. For a given strain increment $\Delta \boldsymbol{\varepsilon}$ within the interval $[t_n, t_{n+1}]$ computed at the nodal points and the known state of the plastic strains $\boldsymbol{\varepsilon}_n^p$ and internal variables $\boldsymbol{\alpha}_n$ at t_n, the updated values $\boldsymbol{\varepsilon}_{n+1}^p$ and $\boldsymbol{\alpha}_{n+1}$ at t_{n+1} are computed.

2.4.1 Basic equations of infinitesimal strain plasticity

Infinitesimal strain plasticity theory is characterized by an additive decomposition of the total strains $\boldsymbol{\varepsilon}$ into elastic $\boldsymbol{\varepsilon}^e$ and plastic $\boldsymbol{\varepsilon}^p$ parts as $\boldsymbol{\varepsilon} = \boldsymbol{\varepsilon}^e + \boldsymbol{\varepsilon}^p$. The stress is expressed in terms of elastic modulus tensor $\mathbf{C}$ and the elastic strain as $\boldsymbol{\sigma} = \mathbf{C} : (\boldsymbol{\varepsilon} - \boldsymbol{\varepsilon}^p)$. The evolution of the plastic strains and the internal plastic variable $\boldsymbol{\alpha}$ is assumed in an associative format:

$$\dot{\boldsymbol{\varepsilon}}^p = \dot{\gamma} \frac{\partial f}{\partial \boldsymbol{\sigma}}, \quad \dot{\alpha} = \dot{\gamma} \frac{\partial f}{\partial \mathbf{q}}. \tag{12}$$

The yield function $f(\boldsymbol{\sigma}, \mathbf{q}) \leq 0$ is expressed in terms of the stresses and the stresslike plastic variable $\mathbf{q}$. Here, $\mathbf{H}$ is the matrix of generalized plastic moduli, which relates $\mathbf{q}$ and $\boldsymbol{\alpha}$ as $\mathbf{q} = -\mathbf{H} : \boldsymbol{\alpha}$. $\dot{\gamma} \geq 0$ is the consistency parameter. The loading/unloading conditions are provided by the Kuhn–Tucker conditions:

$$\dot{\gamma} \geq 0, \quad f(\boldsymbol{\sigma}, \mathbf{q}) \leq 0, \quad \dot{\gamma} f(\boldsymbol{\sigma}, \mathbf{q}) = 0, \quad \dot{\gamma} \dot{f}(\boldsymbol{\sigma}, \mathbf{q}) = 0. \tag{13}$$

2.4.2 Backward Euler integration

Using the backward Euler scheme, the algorithmic forms of Eq. (12) are obtained as [45]

$$\boldsymbol{\varepsilon}_{n+1}^p = \boldsymbol{\varepsilon}_n^p + \Delta \gamma_{n+1} \frac{\partial f_{n+1}}{\partial \boldsymbol{\sigma}_{n+1}}, \quad \boldsymbol{\alpha}_{n+1} = \boldsymbol{\alpha}_n + \Delta \gamma_{n+1} \frac{\partial f_{n+1}}{\partial \mathbf{q}_{n+1}}, \tag{14}$$

with $\Delta \gamma_{n+1} = \dot{\gamma}_{n+1} \Delta t$. The algorithmic form of the Kuhn–Tucker conditions (13) is given as follows:

$$\Delta \gamma_{n+1} \geq 0, \quad f_{n+1} \leq 0, \quad \Delta \gamma_{n+1} f_{n+1} = 0. \tag{15}$$

Using the return map algorithm [44], the trial stress tensor $\boldsymbol{\sigma}_{n+1}^{\text{trial}} = \mathbf{C} : (\boldsymbol{\varepsilon}_{n+1} - \varepsilon_n^p)$ is computed. If $\boldsymbol{\sigma}_{n+1}^{\text{trial}}$ stress is admissible according to Eq. (15), then the step $[t_n, t_{n+1}]$ is treated as elastic. However, if the stress is not admissible, it is projected on the yield surface with the conditions $f_{n+1} = 0$, $\Delta \gamma_{n+1} > 0$ $\Delta \boldsymbol{\varepsilon}_{n+1}^p \neq 0$, $\Delta \boldsymbol{\alpha}_{n+1}^p \neq 0$. The yield condition $f_{n+1} = 0$ and the algebraic set of nonlinear equations (14) are enforced iteratively. At the ith iteration step the residuals of Eq. (14) are given as

$$
\mathbf{R}_{n+1}^{(i)} = \left\{ \begin{array}{c} -\boldsymbol{\varepsilon}_{n+1}^{p(i)} + \boldsymbol{\varepsilon}_n^{\mathrm{p}} + \Delta\gamma_{n+1}^{(i)}\left(\frac{\partial f}{\partial\boldsymbol{\sigma}}\right)_{n+1}^{(i)} \\ -\boldsymbol{\alpha}_{n+1}^{(i)} + \boldsymbol{\alpha}_n + \Delta\gamma_{n+1}^{(i)}\left(\frac{\partial f}{\partial\mathbf{q}}\right)_{n+1}^{(i)} \end{array} \right\} \overset{?}{=} \mathbf{0} \tag{16}
$$

and solved recursively with the initialization of the variables as $i = 0$, $\Delta\gamma_{n+1}^{(0)} = 0$, $\boldsymbol{\varepsilon}_{n+1}^{p(0)} = \boldsymbol{\varepsilon}_n^{\mathrm{p}}$, $\boldsymbol{\alpha}_{n+1}^{(0)} = \boldsymbol{\alpha}_n$. The increment of the consistency parameter is calculated as

$$
\Delta\Delta\gamma^{(i)} = \frac{f_{n+1}^{(i)} - \nabla_C^{\mathrm{T}}\mathbf{A}\mathbf{R}_{n+1}^{(i)}}{\nabla_C^{\mathrm{T}}\mathbf{A}\nabla}, \tag{17}
$$

where $\nabla_C^{\mathrm{T}} = \left[f_{n+1,\boldsymbol{\sigma}}^{(i)} : \mathbf{C} \quad f_{n+1,\mathbf{q}}^{(i)} : \mathbf{H} \right]$, $\nabla = \left[f_{,\boldsymbol{\sigma}} \quad f_{,\mathbf{q}} \right]_{n+1}^{(i)\mathrm{T}}$. With $\mathbb{I}$ as the fourth-order unit tensor, $\mathbf{A}$ is written as

$$
\mathbf{A}^{-1} = \begin{pmatrix} \mathbb{I} + \left(\Delta\gamma f_{,\boldsymbol{\sigma}\boldsymbol{\sigma}}\right)_{n+1}^{(i)} : \mathbf{C} & \left(\Delta\gamma f_{,\boldsymbol{\sigma}\mathbf{q}}\right)_{n+1}^{(i)} : \mathbf{H} \\ \left(\Delta\gamma f_{,\mathbf{q}\boldsymbol{\sigma}}\right)_{n+1}^{(i)} : \mathbf{C} & \mathbb{I} + \left(\Delta\gamma f_{,\mathbf{q}\mathbf{q}}\right)_{n+1}^{(i)} : \mathbf{H} \end{pmatrix}. \tag{18}
$$

The incremental state variables in the ith iteration are obtained as

$$
\left\{ \begin{array}{c} \Delta\boldsymbol{\varepsilon}^{\mathrm{p}} \\ \Delta\boldsymbol{\alpha} \end{array} \right\}_{n+1}^{(i)} = \mathbf{A}\left(\mathbf{R} + \Delta\Delta\gamma \left\{ \begin{array}{c} f_{,\boldsymbol{\sigma}} \\ f_{,\mathbf{q}} \end{array} \right\}\right)_{n+1}^{(i)}. \tag{19}
$$

Finally, the state variables and the consistency parameter are updated until the residual becomes close enough to zero in the Newton–Raphson solution algorithm:

$$
\boldsymbol{\varepsilon}_{n+1}^{p(i+1)} = \boldsymbol{\varepsilon}_{n+1}^{p(i)} + \Delta\boldsymbol{\varepsilon}_{n+1}^{p(i)}, \quad \boldsymbol{\alpha}_{n+1}^{(i+1)} = \boldsymbol{\alpha}_{n+1}^{(i)} + \Delta\boldsymbol{\alpha}_{n+1}^{(i)}, \quad \Delta\gamma^{(i+1)} = \Delta\gamma^{(i)} + \Delta\Delta\gamma^{(i)}. \tag{20}
$$

2.4.3 Consistent elastoplastic tangent moduli

The algorithmic elastoplastic tangent moduli $\mathbf{C}^{\mathrm{ep}} = \partial\boldsymbol{\sigma}_{n+1}/\partial\boldsymbol{\varepsilon}_{n+1}$ are computed at the converged step t_{n+1} as

$$
\mathbf{C}^{\mathrm{ep}} = \mathbf{C} : \mathbf{A}_{\boldsymbol{\varepsilon}\boldsymbol{\varepsilon}} - \frac{\left(\mathbf{C} : \mathbf{A}_{\boldsymbol{\varepsilon}\boldsymbol{\varepsilon}} : f_{,\boldsymbol{\sigma}} + \mathbf{C} : \mathbf{A}_{\boldsymbol{\varepsilon}\boldsymbol{\sigma}} : f_{,\mathbf{q}}\right) \otimes \left(f_{,\boldsymbol{\sigma}} : \mathbf{C} : \mathbf{A}_{\boldsymbol{\varepsilon}\boldsymbol{\varepsilon}} + f_{,\mathbf{q}} : \mathbf{H} : \mathbf{A}_{\boldsymbol{\sigma}\boldsymbol{\varepsilon}}\right)}{\nabla_C^{\mathrm{T}}\mathbf{A}\nabla}, \tag{21}
$$

where $\mathbf{A}_{\boldsymbol{\varepsilon}\boldsymbol{\varepsilon}}$, $\mathbf{A}_{\boldsymbol{\varepsilon}\boldsymbol{\sigma}}$, and $\mathbf{A}_{\boldsymbol{\sigma}\boldsymbol{\varepsilon}}$ are submatrices of the algorithm matrix $\mathbf{A}$.

3 Numerical results

In this section, the developed finite-element formulation and the proposed solution algorithms for elastoplastic analysis of Mindlin plates are applied to selected benchmark analyses and parametric studies. Before presenting the elastoplastic examples, we investigate the accuracy of the computed stresses.

3.1 Simply supported elastic square plate: numerical assessment of the accuracy of stresses

The accuracy of the calculated stresses using the proposed mixed formulation is investigated by comparing the analysis results with analytical results given by Reddy [46] for a simply supported moderately thick square plate with a height-to-length ratio of $h/a = 0.1$ and elastic material behavior. Both sinusoidal (SL) $q(x, y) = q_0\sin(\pi x/a)\sin(\pi y/a)$ and uniformly distributed loading (UL) $q(x, y) = q_0$ cases are considered. It must be pointed out that SL results are exact and UL results are obtained from the first 19 terms of the analytical solution. To ensure a sufficient quality of the discretization, five different finite-element meshes in a range of 4×4 to 20×20 elements were used in a mesh sensitivity study (Table 3). In Table 3, $\overline{w} = 10^2 w_0 D/(a^4 q_0)$ denotes the nondimensional central deflection and $\overline{\sigma}_{xx} = \sigma_{xx}h^2/(a^2 q_0)$, $\overline{\sigma}_{xy} = \sigma_{xy}h^2/(a^2 q_0)$, and $\overline{\sigma}_{xz} = \sigma_{xz}h/(aq_0)$

Table 3 Influence of discretization: nondimensional central deflection and stresses of a simply supported square plate

Load case	Source		$\overline{w}$	$\overline{\sigma}_{xx}$	$\overline{\sigma}_{xy}$	$\overline{\sigma}_{xz}$
SL	Mixed FEM (mesh)	(4×4)	0.2578	0.1805	0.1078	0.2263
		(8×8)	0.2668	0.1876	0.1125	0.2357
		(12×12)	0.2686	0.1889	0.1133	0.2374
		(16×16)	0.2693	0.1894	0.1136	0.2380
		(20×20)	0.2696	0.1896	0.1137	0.2382
		Reddy [46]	0.2702	0.1900	0.1140	0.2387
UL	Mixed FEM (mesh)	(4×4)	0.4392	0.2604	0.2535	0.4643
		(8×8)	0.4310	0.2718	0.2255	0.4938
		(12×12)	0.4283	0.2742	0.2176	0.5007
		(16×16)	0.4273	0.2751	0.2143	0.5033
		(20×20)	0.4268	0.2755	0.2126	0.5045
		Reddy [46]	0.4259	0.2762	0.2085	0.4909

$\upsilon = 0.25, \overline{\sigma}_{xx}(a/2, a/2, h/2), \overline{\sigma}_{xy}(a, a, -h/2), \overline{\sigma}_{xz}(0, a/2, 0)$

are nondimensional stress components. The maximum stresses were evaluated at three points: $\overline{\sigma}_{xx}(a/2, a/2, h/2)$, $\overline{\sigma}_{xy}(a, a, -h/2), \overline{\sigma}_{xz}(0, a/2, 0)$. A rapid convergence of the displacements and stress components with an increasing element number is apparent from Table 3. Even for very coarse meshes, the results from the mixed formulation are consistent with the analytical results of Reddy [46]. For the 4×4 mesh and a SL load case an error of ~5% is obtained for both displacement and stress components. This error decreases to 0.20~0.26% (with exact results) for the finest mesh with 20×20 elements. For the same mesh configuration $[\overline{\sigma}_{xx}(a/2, a/2, h/2)$ elements] and load case UL, the errors for $\overline{w}, \overline{\sigma}_{xx}, \overline{\sigma}_{xy}$, and $\overline{\sigma}_{xz}$ are 0.21, 0.25, 1.97, and 2.77% (with analytical results of the first 19 terms), respectively. One may conclude that the results of the presented mixed finite-element formulation show a parallel behavior, are close enough to the exact results, and can predict the transverse shear stresses quite accurately, although a first-order shear deformation theory with linear shape functions is employed.

3.2 Elastoplastic plate with linear hardening

A uniformly loaded simply supported square plate (6 m × 6 m) with thickness $h = 0.2$ m is considered. The elastic modulus of the plate, the Poisson's ratio, and the yield stress are assumed as $E = 2.067 \times 10^8$ MPa, $\upsilon = 0.3$, and $\sigma_Y = 206.7 \times 10^3$ kPa. Linear hardening is assumed, with a tangent modulus $E_T = 2.067 \times 10^6$ MPa. The hardening modulus H and E_T are related as $H = E_T/(1 - E_T/E)$ [22]. For comparison, the results from element-free Galerkin analysis by Belinha and Dinis [47] are used, where a layered approach was adopted with eight layers of equal thickness through the plate cross-section. They used a fine discretization with a regular mesh with 441 nodes, employing seventh-order splines for test functions and 6×6 integration points inside each nodal cell.

To examine the performance of the proposed solution procedure, several parametric studies are performed: four different meshes ($4 \times 4, 8 \times 8, 12 \times 12, 20 \times 20$) and four different configurations of layers across the height (4, 8, 12, 16) and four different numbers of load step (5, 10, 20, 40). In the following diagrams, the nondimensional central deflection of the plate with the plastic moment $M_p = \sigma_Y h^2/4$ is plotted versus the nondimensional loading parameter.

Figure 4 depicts the central deflection of the plate discretized by a coarse mesh consisting of 4×4 elements. The results show that all curves are significantly below the reference curve denoted by a solid line with an average mean square error (AMSE) of 0.836, 1.142, 2.934, and 2.385 for the solution with 4 layers and 1.390, 1.082, 0.885, and 0.778 for the solution obtained with 16 layers. When 20 or 40 loading steps are used, a difference between the results using 4 layers and the remaining results using 8 and more layers is observed.
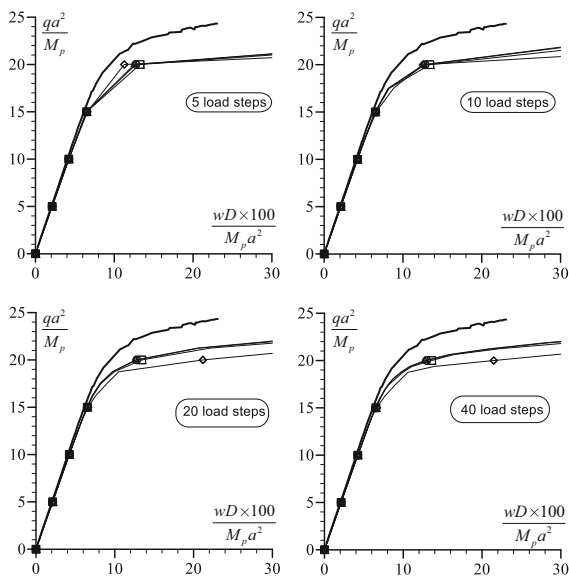
Fig. 4 Central deflection of a simply supported elastoplastic square plate with 4×4 mesh. *Thick line* Belinha and Dinis [47], *diamond* 4 layers, *square* 8 layers, *circle* 12 layers, *triangle* 16 layers
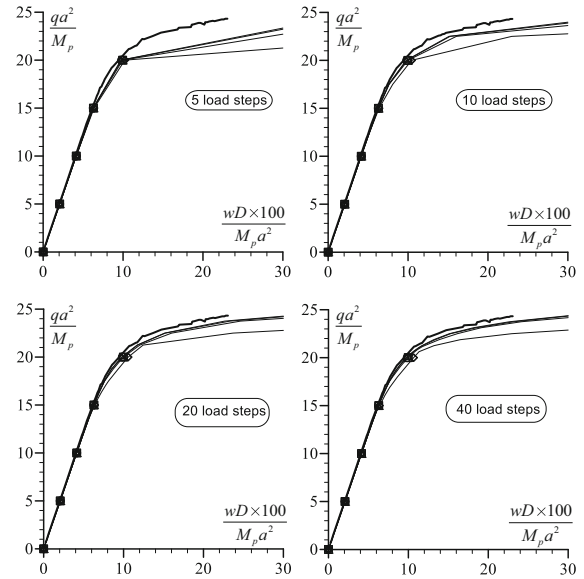
Fig. 5 Central deflection of a simply supported elastoplastic square plate with 8×8 mesh. *Thick line* Belinha and Dinis [47], *diamond* 4 layers, *square* 8 layers, *circle* 12 layers, *triangle* 16 layers

The load–displacement curves for a finer finite-element mesh (8×8) are presented in Fig. 5. For this mesh configuration, the importance of the number of layers for the reflecting nonlinear behavior becomes apparent even for small load steps compared to the 4×4 mesh configuration.

Figure 6 contains the load–displacement diagrams for a discretization using a mesh of 20×20 elements. Based on this figure, it is concluded that, even for a fine discretization, 5 load steps using only 4 layers through the thickness are insufficient and that a sufficient convergence can be achieved with 12 layers and 20 load steps for the present benchmark example.

For further investigation of the convergence behavior of the proposed numerical solution procedure, the AMSEs of the central deflection of the elastoplastic plate with respect to the results obtained from Belinha and Dinis [47] are presented in Fig. 7. It must be noted that the results from Belinha and Dinis are obtained by digitizing the plots from their figures. In Fig. 7 the AMSE is plotted versus the NDOF for different meshes, numbers of layers, and loading steps. The figure shows that the number of layers has a significant effect on the error, while the number of load steps is less significant.

3.3 Elastoplastic analyses of Mindlin plates with perfect plastic constitutive behavior

In this subsection, a parametric study and convergence study for the elastoplastic analysis of a square Mindlin plate is presented for the perfect plasticity case, adopting results from Owen and Hinton [22] as a reference solution that were obtained from the heterosis element [48]. A simply supported and uniformly loaded square plate with nondimensional parameters $a = 1$, $E = 10.92$, $\upsilon = 0.3$, $h = 0.01$, and $\sigma_Y = 1600$ is investigated. From Owen and Hinton [22] we get the central deflections of the plate for both layered and nonlayered analyses. The plate is analyzed with the proposed mixed finite-element formulation using 4 layers, 8 layers, 12 layers, and 16 layers. In Figs. 8 and 9 the nondimensional loading parameters are plotted against nondimensional central deflections for 8×8 and 20×20 finite-element meshes and different numbers of loading steps.

Figure 8 indicates that even for a ratio of $h/a = 0.01$ considering four layers through the thickness is insufficient. From Fig. 9 it is concluded that for the 20×20 mesh, a parallel behavior with the reference result presented in
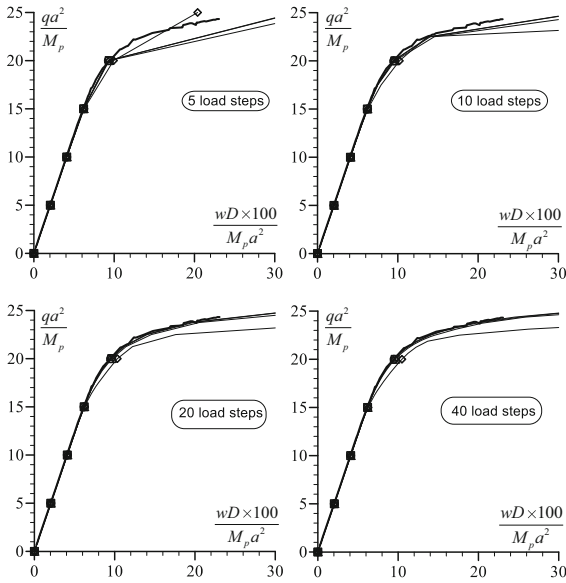
Fig. 6 Central deflection of a simply supported elastoplastic square plate with 20×20 mesh. *Thick line* Belinha and Dinis [47], *diamond* 4 layers, *square* 8 layers, *circle* 12 layers, *triangle* 16 layers
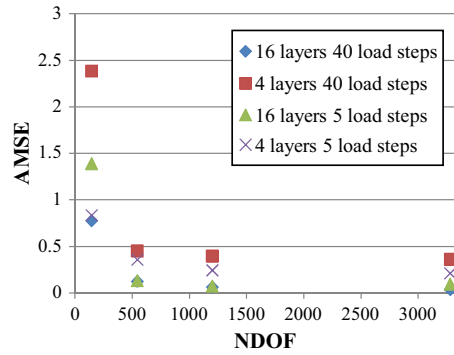

Fig. 7 Average mean square errors of central deflection with respect to results of Belinha and Dinis [47] as a function of the number of degrees of freedom for different numbers of layers and load steps
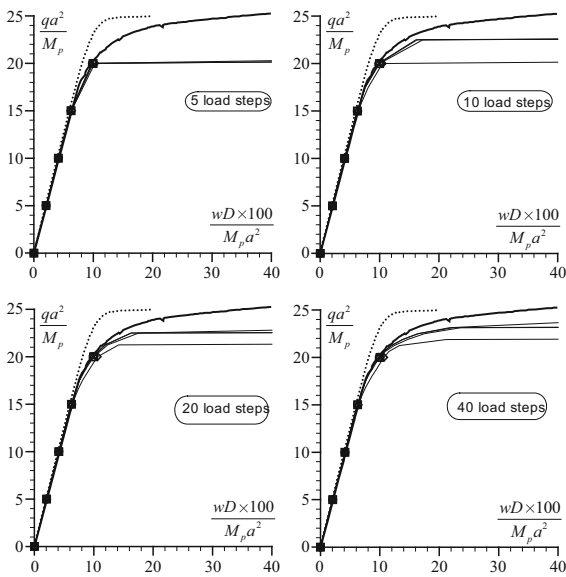

Fig. 8 Central deflection of a simply supported perfectly elastoplastic square plate with 8×8 mesh. *Thick line* Owen and Hinton [22] layered approach, *dotted line* Owen and Hinton [22] nonlayered approach, *diamond* 4 layers, *square* 8 layers, *circle* 12 layers, *triangle* 16 layers
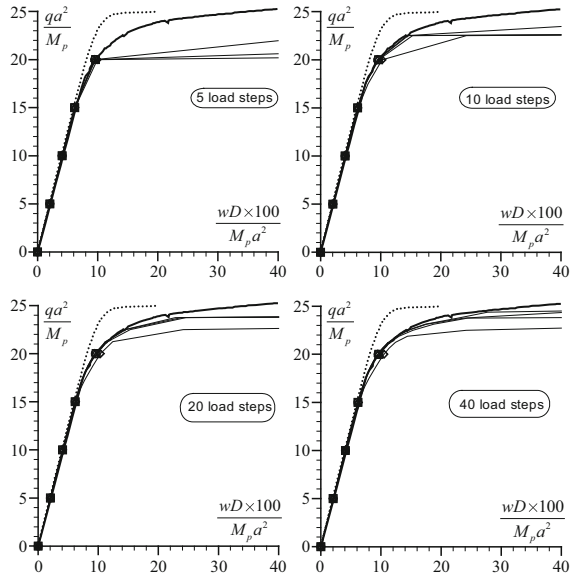

Fig. 9 Central deflection of a simply supported perfectly elastoplastic square plate with 20×20 mesh. *Thick line* Owen and Hinton [22] layered approach, *dotted line* Owen and Hinton [22] nonlayered approach, *diamond* 4 layers, *square* 8 layers, *circle* 12 layers, *triangle* 16 layers

Table 4 Nondimensional central deflection ($w_0 D \times 100/(M_p a^2)$) of a square plate with various thickness-to-width ratios

	qa^2/M_p	4 Layers	8 Layers	12 Layers	16 Layers
$h/a = 0.05$	16.875	7.5519	7.2039	7.1520	7.1368
	20.000	10.5311	9.6917	9.5543	9.4902
	23.125	26.4713	17.3260	16.4164	16.2241
$h/a = 0.10$	16.875	7.8266	7.4664	7.4176	7.4115
	20.000	10.8547	10.0122	9.8840	9.8230
	23.125	27.8144	17.9182	16.9719	16.8071
$h/a = 0.15$	16.875	8.2509	7.9121	7.8755	7.8846
	20.000	11.3736	10.5586	10.4396	10.3938
	23.125	29.8535	18.9286	17.9670	17.8755

Owen and Hinton [22] is obtained when the number of layers is larger than 4 and the number of loading steps is sufficiently large (i.e., larger than 20) to resolve the complete load–displacement diagram.

3.4 Investigation of spatial resolution of plastic zones through the thickness

In this example, the spatiotemporal evolution of plastic deformations through the plate thickness is investigated. To this end the simply supported square plate analyzed in Sect. 3.2 is considered with the same loading, material, and hardening properties. With a side length of $a = 6$ m, three different thickness-to-side-length ratios, $h/a = 0.05, 0.10, 0.15$, are examined. Table 4 contains the nondimensional central deflection of a square plate for three nondimensional load levels (16.875, 20, and 23.125). Four different layer configurations are considered (4, 8, 12, and 16 layers through the plate thickness). It is observed from Table 4 that the influence of the number of layers is increasing with a decreasing h/a ratio and that with an increasing load level, a larger number of layers is required.

Finally, the distribution of the nondimensional normal stress component (σ_{xx}/σ_Y) through the plate thickness at the center of the plate is plotted in Fig. 10 for three different load levels and for two different thickness-to-width ratios. Four and 16 layers are employed to discretize the cross section of the plate. It is observed that the number of layers has a larger effect at larger load levels. Only marginal differences are observed for the two ratios $h/a = 0.05$ and 0.15.

3.5 Investigation of circular, skew, and L-shaped plates

To evaluate the behavior of the proposed finite element in a numerical analysis of plates characterized by non-rectangular shapes subjected to distributed and point loading, a circular plate, a skew, and an L-shaped plate are analyzed in this subsection (Fig. 11). According to the previous convergence studies, the analyses are performed by considering 40 loading steps and 16 layers through the plate section. A constant Poisson's ratio $\upsilon = 0.3$ is used; a plate thickness ratio of $h/a = 0.05$ is assumed unless stated otherwise. Except for the L-shaped plate, the plate boundaries are considered to be clamped. The specific boundary conditions of the L-shaped plate are depicted in Fig. 11. Perfect plasticity is assumed in order to compare the results with existing results from limit load analyses in the literature.

The nondimensional central deflection of a circular plate subjected to uniformly distributed loading is shown in Fig. 12 for three different finite-element discretizations. In the figure, the limit load [17] is also included. Even for a coarse mesh composed of 12 quadrilateral elements over the full plate, a good approximation is achieved.

Owing to the nature of the proposed formalism, point loads cannot be directly employed in the analyses. Similar to the other field variables, shear forces are also continuously distributed over the discretized domain and a concentrated
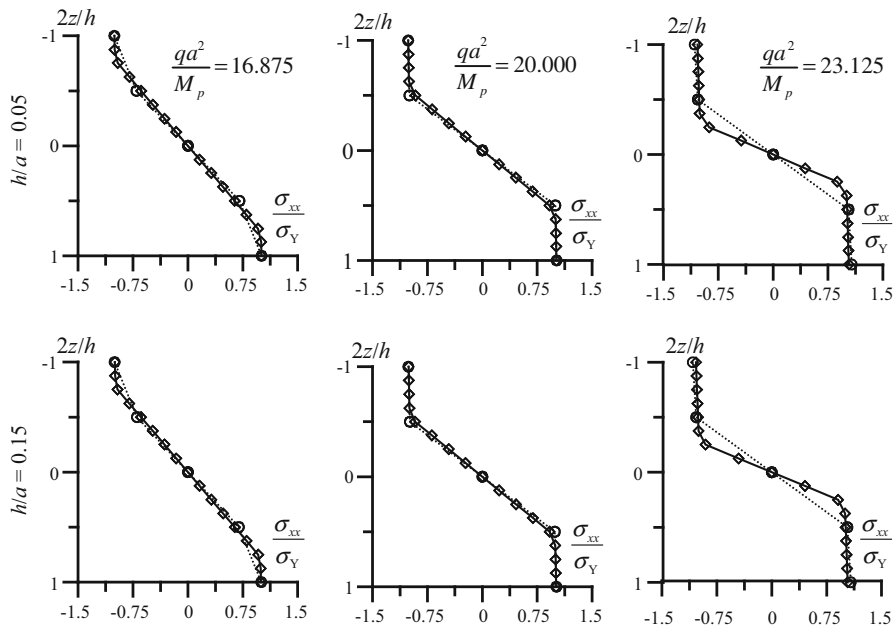
Fig. 10 Distribution of nondimensional normal stress component σ_{xx}/σ_Y through plate thickness at center of plate; *circle* 4 layers, *diamond* 16 layers
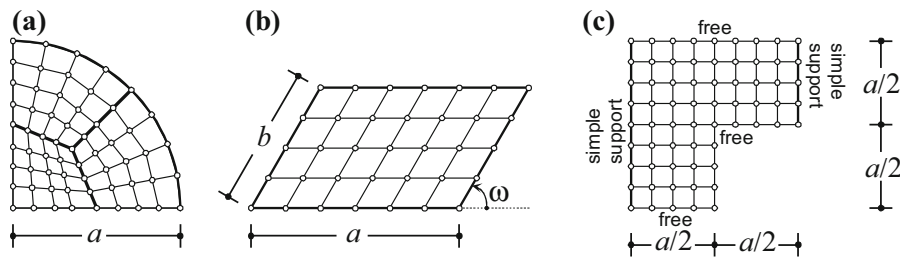

Fig. 11 Geometric properties and representative meshes for plates with various geometries. **a** Quarter of a circular plate. **b** Skew plate. **c** L-shaped plate with boundary conditions

force causes violation of the continuity in shear force parameters. Therefore, point loading requires distributing the force over a small plate element. With this approach the nondimensional central deflection of a circular plate under the action of a central point load P is presented in Fig. 13. The point load P is considered to be distributed over a square area $0.04a \times 0.04a$, where a is the radius of the circular plate. It can be concluded that both for point loading and uniform loading a similar number of elements is required to obtain converged values of the central deflection.

Figure 14 presents the nondimensional central deflection of a skew plate with side length ratio $a/b = 1.5$ and angle $\omega = 60°$ (Fig. 11) for uniform loading. Convergence of the parameters with respect to the increased element numbers can be observed from the figure. The results converge very rapidly and are consistent with the limit load value provided by Sobotka [18].

The last problem is concerned with an L-shaped plate. At two opposite edges the boundary is assumed to be simply supported while all other boundaries are assumed to be free (Fig. 11). The uniformly loaded plate is discretized with four different meshes. As a benchmark result, the limit load provided by Bleyer et al. [19] is used for comparison. Figure 15 depicts the nondimensional displacement of the reentrant corner of the L-shaped plate. A difficulty in the achievement of the convergence is observed because this problem involves a stronger singularity than previous
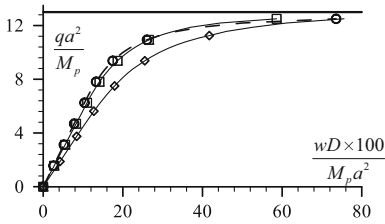
Fig. 12 Central deflection of a clamped circular plate subjected to uniformly distributed load. *Thick line* limit load (Hopkins and Wang [17]), *diamond* 12 elements, *square* 48 elements, *circle* 108 elements
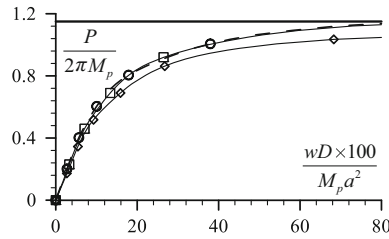

Fig. 13 Central deflection of a clamped circular plate subjected to central point load. *Thick line* limit load (Hopkins and Wang [17]), *diamond* 15 elements, *square* 51 elements, *circle* 111 elements
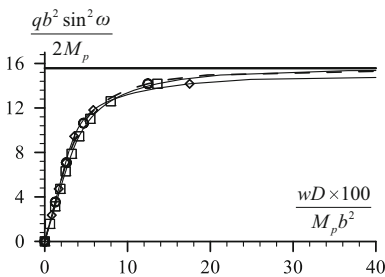

Fig. 14 Central deflection of a clamped skew plate subjected to uniformly distributed load. *Thick line* limit load (Sobotka [18]), *diamond* 4 × 6 elements, *square* 8 × 12 elements, *circle* 12 × 18 elements
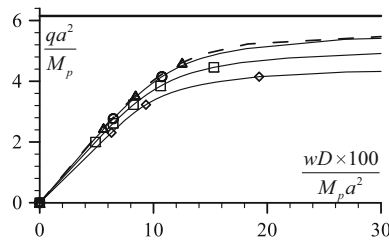

Fig. 15 Deflection of reentrant corner of L-shaped plate subjected to uniformly distributed load. *Thick line* limit load (Bleyer et al. [19]), *diamond* 48 elements, *square* 108 elements, *circle* 363 elements, *triangle* 588 elements

problems. There is a slight difference between the limit load given by Bleyer et al. [19] and the maximum load reached by this procedure.

3.6 Investigation of element behavior for mesh distortion

To investigate the mesh sensitivity of the proposed element, the linear static problem presented in [49] is studied. For this purpose a clamped square plate with $h/a = 0.001$ and $\upsilon = 0.3$ is considered. Owing to the symmetry of the problem, a quarter of the uniformly loaded plate is considered. The distorted meshes (Fig. 16) are generated by moving the position of the interior nodal points by a factor s [49]. Based on a regular mesh, the new coordinates (x', y') of the interior points are obtained from the initial coordinates (x, y) using the following formulas:

$$x' = x + r_c s \Delta x, \quad y' = y + r_c s \Delta y, \tag{22}$$

where r_c is a randomly generated number between -1.0 and 1.0, $s \in [0, 0.5]$ is used to control the order of distortion, and Δx and Δy correspond to the initial sizes of the regular mesh elements in the x- and y-directions, respectively. The yellow regions in Fig. 16 show that the related element is no longer convex. Table 5 contains the nondimensional central deflection of the plate for three different values of s. This table also contains the deviation κ of the results from distorted meshes as compared to regular mesh layouts obtained from the proposed mixed finite-element formulation for different levels of mesh distortion expressed by the parameter s. As a means of comparison, the respective deviations reported in [49] for different plate elements are included in this table. Similar as the finite element based on the assumed natural strain method proposed by Bathe and Dvorkin [50] (MITC element) and in contrast to the finite elements with mixed interpolation and smoothed curvatures (MISC elements), the deviation κ increases as the irregularity parameter s increases. However, for $s = 0.5$, the deviation is considerably smaller
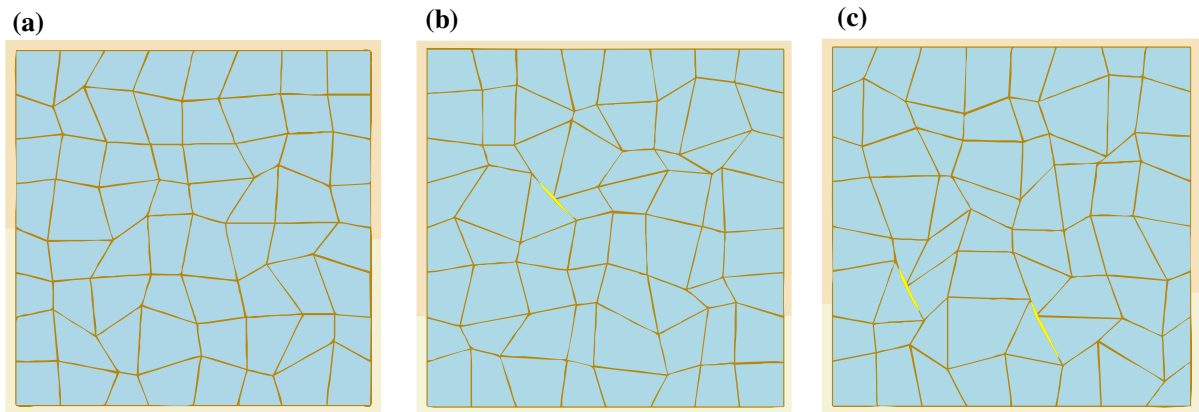
(a)   **(b)**   **(c)**

Fig. 16 Distorted meshes of a quarter of a square plate: **a** $s = 0.2$; **b** $s = 0.4$; **c** $s = 0.5$

Table 5 Nondimensional central deflection $w_0 100 D/(qa^4)$ of a clamped plate under uniform load for various distorted meshes and the deviation κ of results from one of the distorted meshes with respect to the regular mesh layouts

Element	$s = 0.0$	$s = 0.2$	κ (%)	$s = 0.4$	κ (%)	$s = 0.5$	κ (%)
MITC4	0.1211	0.1245	2.8	0.1189	1.8	0.1087	10.2
MISC1	0.1302	0.1361	4.5	0.1377	5.8	0.1347	3.5
MISC2	0.1266	0.1323	4.5	0.1331	5.1	0.1287	1.7
MISC3	0.1249	0.1305	4.5	0.1309	4.8	0.1260	0.9
MISC4	0.1233	0.1287	4.4	0.1288	4.5	0.1227	0.5
Mixed element	0.1334	0.1301	2.5	0.1294	3.0	0.1290	3.3
Exact solution	0.1265	0.1265		0.1265		0.1265	

For comparison, solutions from existing finite elements [49] are included

for the mixed element as compared to the MITC element. In average, it concluded that the current element shows a sensitivity to the mesh distortion that is comparable to (and in general smaller than) the other plate elements.

4 Conclusions

The main objective of this article was to develop a new mixed finite-element formulation for elastoplastic structural analysis with a specific application to Mindlin plates. The proposed nonlinear finite-element model preserves stress parameters as field variables beside displacement type field variables, during the whole solution procedure. The proposed formulation for Mindlin plates does not suffer from shear locking even without using any stabilization procedure.

The formulation provides both displacement and stress increments directly at the nodal points. The strain increments are computed from stress increments in terms of linear constitutive relations. The local integration of constitutive equations is performed at nodal points instead of Gaussian points based on the updated continuous strain field. The proposed algorithmic formulation for elastoplastic analysis of isotropic Mindlin plates is characterized by employing an implicit integration of 3D elastoplastic models. A layered approach is adopted for the spatial resolution of plastic deformations through the plate thickness.

The finite-element plate model was applied to numerical analyses of plates characterized by perfectly plastic and linear hardening elastoplastic material behavior and the von Mises criterion. It was shown that quadrilateral C^0 plate finite elements were able to perform well in elastoplastic analyses even for moderate discretizations. Even in

the case of coarse meshes, the nonlinear solution process showed stable convergence through the complete iterative procedure. It was demonstrated in comparative analyses that the current plate element also performs well in the case of circular, skew, and other types of geometries and that the results show only a slight sensitivity with respect to mesh distortion.

In a number of parametric studies, the applicability and accuracy of the developed formulation were investigated for different spatial discretizations, loading steps, and numbers of layers. From these benchmark analyses it is concluded that even for thin plates a minimum of four layers across the thickness of the plates are required to accurately replicate the elastoplastic behavior. For increasing load levels, the number of layers must be increased to preserve the accuracy of the analysis. Obviously, the number of layers strongly affects the error level, while the number of load steps affects the accuracy only slightly.

References

1. Zienkiewicz OC, Taylor RL, Fox DD (2014) The finite element method for solid and structural mechanics, 7th edn. Butterworth-Heinemann, Oxford
2. Bathe K-J (1996) Finite element procedures. Prentice Hall, Upper Saddle River
3. Doğruoğlu AN, Omurtag MH (2000) Stability analysis of composite-plate foundation interaction by mixed FEM. J Eng Mech ASCE 126:928–936
4. Kutlu A, Omurtag MH (2012) Large deflection bending analysis of elliptic plates on orthotropic elastic foundation with mixed finite element method. Int J Mech Sci 65:64–74
5. Omurtag MH, Aköz AY (1995) Isoparametric mixed finite element formulation of orthotropic cylindrical shells. Comput Struct 55:915–924
6. Putcha NS, Reddy JN (1986) A refined mixed shear flexible finite element for the nonlinear analysis of laminated plates. Comput Struct 22:529–538
7. Wisniewski K, Turska E (2012) Four-node mixed Hu–Washizu shell element with drilling rotation. Int J Numer Methods Eng 90:506–536
8. Papachristidis A, Fragiadakis M, Papadrakakis M (2010) A 3D fibre beam-column element with shear modelling for the inelastic analysis of steel structures. Comput Mech 45:553–572
9. Soydas O, Saritas A (2013) An accurate nonlinear 3d Timoshenko beam element based on Hu–Washizu functional. Int J Mech Sci 74:1–14
10. Tort C, Hajjar JF (2009) Mixed finite-element modeling of rectangular concrete-filled steel tube members and frames under static and dynamic loads. J Struct Eng 136:654–664
11. Wackerfuß J, Gruttmann F (2011) A nonlinear Hu–Washizu variational formulation and related finite-element implementation for spatial beams with arbitrary moderate thick cross-sections. Comput Methods Appl Mech Eng 200:1671–1690
12. Taylor RL, Filippou FC, Saritas A, Auricchio F (2003) A mixed finite element method for beam and frame problems. Comput Mech 31:192–203
13. Hjelmstad KD, Taciroglu E (2002) Mixed methods and flexibility approaches for nonlinear frame analysis. J Constr Steel Res 58:967–993
14. Saritas A, Soydas O (2012) Variational base and solution strategies for non-linear force-based beam finite elements. Int J Non-Linear Mech 47:54–64
15. Nukala PKVV, White DW (2004) Variationally consistent state determination algorithms for nonlinear mixed beam finite elements. Comput Methods Appl Mech Eng 193:3647–3666
16. Freiberger W, Tekinalp B (1956) Minimum weight design of circular plates. J Mech Phys Solids 4:294–299
17. Hopkins HG, Wang AJ (1955) Load-carrying capacities for circular plates of perfectly-plastic material with arbitrary yield condition. J Mech Phys Solids 3:117–129
18. Sobotka Z (2013) Theory of plasticity and limit design of plates. Elsevier, Amsterdam
19. Bleyer J, Van Le C, de Buhan P (2015) Locking-free discontinuous finite elements for the upper bound yield design of thick plates. Int J Numer Methods Eng. doi:10.1002/nme.4912
20. Eggers H, Kröplin B (1978) Yielding of plates with hardening and large deformations. Int J Numer Methods Eng 12:739–750
21. Dinis LMS, Owen DRJ (1978) Elastic–viscoplastic analysis of plates by the finite element method. Comput Struct 8:207–215
22. Owen DRJ, Hinton E (1980) Finite elements in plasticity: theory and practice. Pineridge Press, Swansea
23. Bathe K, Bolourchi S (1980) A geometric and material nonlinear plate and shell element. Comput Struct 11:23–48
24. Dinis LMS, Owen DRJ (1982) Elasto-viscoplastic and elasto-plastic large deformation analysis of thin plates and shells. Int J Numer Methods Eng 18:591–607

25. Reddy BD, Mitchell GP (1983) The analysis of elastic–plastic plates: a quadratic programming problem and its solution by finite elements. Comput Methods Appl Mech Eng 41:237–248
26. Wempner G, Chao-Meng H (1984) A simple model of elastic–plastic plates. Int J Solids Struct 20:77–80
27. Papadopoulos P, Taylor RL (1990) Elasto-plastic analysis of Reissner–Mindlin plates. Appl Mech Rev 43:S40–S50
28. Daye MA, Toridis TG (1991) Elasto-plastic algorithms for plates and shells under static and dynamic loads. Comput Struct 39:195–205
29. Papadopoulos P, Taylor RL (1991) An analysis of inelastic Reissner–Mindlin plates. Finite Element Anal Des 10:221–233
30. Ibrahimbegović A, Frey F (1993) An efficient implementation of stress resultant plasticity in analysis of Reissner–Mindlin plates. Int J Numer Methods Eng 36:303–320
31. Auricchio F, Taylor RL (1994) A generalized elastoplastic plate theory and its algorithmic implementation. Int J Numer Methods Eng 37:2583–2608
32. Croce LD, Venini P, Nascimbene R (2003) Numerical simulation of an elastoplastic plate via mixed finite elements. J Eng Math 46:69–86
33. Rabczuk T, Areias PMA, Belytschko T (2007) A meshfree thin shell method for non-linear dynamic fracture. Int J Numer Methods Eng 72:524–548
34. Areias P, Rabczuk T (2013) Finite strain fracture of plates and shells with configurational forces and edge rotations. Int J Numer Methods Eng 94:1099–1122
35. Areias P, Rabczuk T, César de Sá JM, Garção JE (2015) Finite strain quadrilateral shell using least-squares fit of relative Lagrangian in-plane strains. Finite Elem Anal Des 98:26–40
36. Liu GR, Nguyen-Thoi T, Lam KY (2008) A novel alpha finite element method (αFEM) for exact solution to mechanics problems using triangular and tetrahedral elements. Comput Methods Appl Mech Eng 197:3883–3897
37. Thai-Hoang C, Nguyen-Thanh N, Nguyen-Xuan H, Rabczuk T (2011) An alternative alpha finite element method with discrete shear gap technique for analysis of laminated composite plates. Appl Math Comput 217:7324–7348
38. Thai CH, Ferreira AJM, Bordas SPA, Rabczuk T, Nguyen-Xuan H (2014) Isogeometric analysis of laminated composite and sandwich plates using a new inverse trigonometric shear deformation theory. Eur J Mech A Solids 43:89–108
39. Omurtag MH, Aköz AY (1993) A compatible cylindrical shell element for stiffened cylindrical shells in a mixed finite element formulation. Comput Struct 49:363–370
40. De Souza RM (2000) Force-based finite element for large displacement inelastic analysis of frames. Doctoral Dissertation, University of California, Berkeley
41. Ugural AC, Fenster SK (2003) Advanced strength and applied elasticity. Prentice Hall, Upper Saddle River
42. Voyiadjis GZ, Woelke P (2008) Elasto-plastic and damage analysis of plates and shells. Springer, Berlin
43. Ortiz M, Popov EP (1985) Accuracy and stability of integration algorithms for elastoplastic constitutive relations. Int J Numer Methods Eng 21:1561–1576
44. Simo JC, Hughes TJR (1998) Computational inelasticity. Springer, New York
45. Meschke G (2011) Finite element method for nonlinear analysis of inelastic materials and structures. Lecture Notes. Institute for Structural Mechanics—Ruhr-University Bochum, Bochum
46. Reddy JN (2006) Theory and analysis of elastic plates and shells. CRC Press, Boca Raton
47. Belinha J, Dinis LMJS (2006) Elasto-plastic analysis of plates by the element free Galerkin method. Eng Comput 23:525–551
48. Hughes TJR, Cohen M (1978) The "heterosis" finite element for plate bending. Comput Struct 9:445–450
49. Nguyen-Xuan H, Rabczuk T, Bordas S, Debongnie JF (2008) A smoothed finite element method for plate analysis. Comput Methods Appl Mech Eng 197:1184–1203
50. Bathe K, Dvorkin EN (1985) A four-node plate bending element based on Mindlin/Reissner plate theory and a mixed interpolation. Int J Numer Methods Eng 21:367–383